PLASMA ASSISTED CVD OF THICK YTTRIA PARTIALLY STABILIZED ZIRCONIA COATINGS

S. Chevillard
S. Drawin
M.H. Vidal-Sétif

ONERA - Materials Science Department
BP 72
92322 CHATILLON CEDEX
FRANCE

SUMMARY

Plasma-assisted chemical vapor deposition has been successfully used to deposit thick (20 - 150 µm) zirconia - (5-20wt%) yttria coatings on metallic and alumina substrates, with high rates (up to 150 µm/h) at temperatures ranging from 400 to 750°C. Tetrachloride ($ZrCl_4$) and $Y(thd)_3$ β-diketonate were used as zirconium and yttrium source materials. Vaporization conditions have been studied for both precursors. Morphology, impurity content and crystallographic structure of the coatings were investigated. At all deposition temperatures, the coatings exhibited columnar morphology and {100} crystallographic texture. At low substrate temperature (400°C), the pore volume fraction was high (*ca.* 50%) and the coatings incorporated some carbon and chlorine impurities, but at high temperature (750°C), the pore fraction reduced to about 25% and little carbon and no chlorine were detected. Metastable tetragonal « t' » phase was the main constituent of coatings with 7 and 10wt% yttria. Annealing for 24 and 120 hours of ZrO_2 - 7wt% Y_2O_3 coating deposited at 400°C showed that cubic phase with an yttria content of about 11wt% is allowed to form, at the expense of the « t' » phase whose yttria content diminishes to 4wt%. This relatively fast evolution towards thermodynamic equilibrium may be related to the high porosity level.

1. INTRODUCTION

The use of thermal barrier coatings (TBCs) cannot be currently by-passed for the enhancement of both aeronautical and industrial gas turbine performance and efficiency. Zirconia-based compositions, and especially 6-8wt% yttria partially stabilized zirconia, are widely used, because of an outstanding behaviour at high temperature (high chemical and structural stability, high coefficient of thermal expansion, low thermal conductivity) and a good resistance to thermal cycling [1].

Numerous depositions techniques of zirconia-based films are reported in the literature, including :

- sol-gel processing [2],
- chemical vapor deposition (CVD) : conventional thermal CVD [3], metal-organic CVD (MOCVD) [4], plasma-enhanced (or assisted) CVD (PECVD or PACVD) [5], electrochemical vapor deposition (EVD) [6], combustion CVD (CCVD) [7],
- physical vapor deposition (PVD) : sputtering [8], laser PVD [9], electron beam PVD (EBPVD) [10], and
- plasma spraying [11],

for numerous applications : TBCs for gas turbine engines [12, 13], stationary gas turbines [14] and diesel engines [15], solid electrolytes for fuel cells [16], gas sensors [5], insulating layers for semiconductors, buffer layers for YBaCuO supraconductors, hard coatings, optical coatings, *etc.* But few techniques are suited for thick (150 to 300 µm) coatings, which require high deposition rates, as needed for TBCs.

Plasma spraying and EBPVD are currently the only processes used in production for TBCs [17, 18]. Yet being typically line-of-sight processes, they are limited to the coating of simple-shaped airfoils, and deposition on shadowed regions of multiple airfoils may be very difficult [19]. A non-directive alternative deposition process would present definite advantages in this respect.

CVD techniques are in that sense well fitted. EVD allows deposition rates as high as 100 µm/h [16] but requires porous substrates, and too low deposition rates (typically 1 µm/h) exclude thermal CVD. Plasma activation, at either radio (13.56 MHz) or microwave (2.45 GHz) frequencies, has been widely used for the deposition of various layers in microelectronics, hard coatings and oxide diffusion barriers [20]. It presents two benefits : lowering of the substrate temperature, in some cases down to less than 100°C, and enhancement of the deposition rate by up to two orders of magnitude.

Moreover, PECVD processes allow to vary the coating morphology ; in the particular case of zirconia-based coatings *columnar* morphologies can be obtained, as already shown by Cao [5] for zirconia-yttria solid solutions and Bertrand [21, 22] and Gavillet [23] for pure zirconia. Compared to the lamellar morphology of plasma-sprayed coatings, the columnar morphology is generally preferred for cycled applications at high temperature as in gas turbine engines [19]. The improved strain tolerance is due to the orientation of the intercolumnar porosity perpendicular to the

Paper presented at an AGARD SMP Meeting on "Thermal Barrier Coatings", held in Aalborg, Denmark, 15-16 October 1997, and published in R-823.

substrate/coating interface, thus allowing contraction and expansion without cracking.

This paper presents the work in progress at ONERA to develop a PECVD process for the deposition of yttria partially stabilized zirconia thermal barrier coatings. Electrodeless microwave plasma generation has been preferred to radio-frequency, because of the potentially higher electron densities involved (10^{17} - 10^{18} m^{-3}) and thus higher active species densities and higher deposition rates.

2. EXPERIMENTAL DETAILS

All deposits were performed in a home-built laboratory-scale reactor based on the apparatus used by Bertrand [21, 22]. The reactor can schematically be decomposed into four parts (Figure 1) [24]:

- the gas generation and distribution system allows the vaporization of the zirconium and yttrium solid precursors and their transport, together with argon carrier gas and oxygen, to the deposition chamber ;
- the deposition chamber is a 100 mm in diameter, 280 mm long quartz tube. It is surrounded by a microwave cavity (180 mm in diameter) coupled through a waveguide to a 1200 W maximum power 2.45 GHz microwave generator ;
- the substrate (20 mm in diameter, 2 mm thick) is placed on a temperature-controlled holder resistively heated by a Ni-Cr wire connected to a 600 VA power supply. The substrate temperature, T_S, can reach a maximum of 1000°C for short durations, but this has to be reduced to 750°C for longer durations due to the rapid oxidation of the Ni-Cr wire at high temperature and low pressure. The distance from the injection nozzle to the substrate can be varied. Substrates are metallic (NiCoCrAlY, preoxidized at 1100°C to allow the growth of an adherent alumina film) or ceramic (sintered α-alumina) ; a hole is drilled on the sample side so that a thermocouple can be introduced to monitor the sample temperature ;
- the gases are evacuated by a Roots blower (Alcatel, 150 $m^3 h^{-1}$) connected to a primary pump (Alcatel, 33 $m^3 h^{-1}$). Corrosive gases are condensed in a liquid nitrogen trap. The total pressure in the deposition chamber is controlled by a throttle valve and a Baratron gauge.

Airtightness is obtained using conventional Viton® O-ring seals, except for the gas generation part which is heated up to 250°C where Kalrez® seals were used. All metallic parts are made of AISI 316 L stainless steel.

Experimental conditions for the deposition of ZrO_2-Y_2O_3 TBC coatings are given in Table 1.

2.1 Zr and Y source materials

Since neither mineral nor metal-organic zirconium and yttrium compounds are gaseous at room temperature, condensed source materials have to be used and vaporized in a specific manner (bubbler, furnace, *etc*).

The precursors for Zr and Y were chosen from literature data and specific investigations were conducted on some

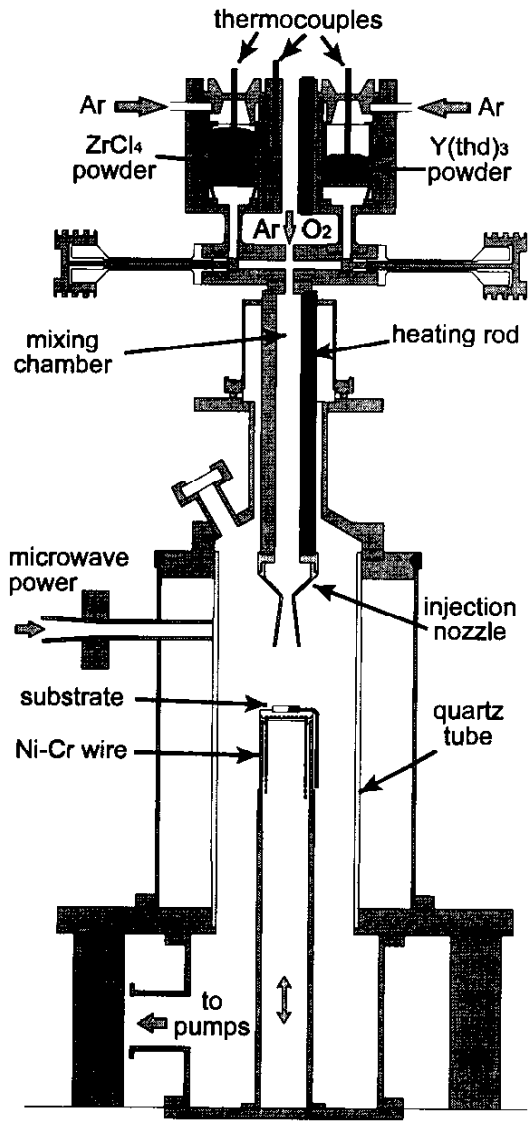

Figure 1 - Apparatus for PECVD of ZrO_2 - Y_2O_3 thermal barrier coatings.

of them [24, 25]. The main selection criteria were :

- a high vapor pressure to ensure high deposition rates (this requirement is less stringent for the Y precusor, because the aimed Y:Zr atomic concentration ratio in the coatings is always less than 1:5) ;
- a good chemical and thermal stability ;
- low toxicity, low moisture sensitivity, low cost.

Zirconium tetrachloride ($ZrCl_4$) and $Y(O_2C_{11}H_{19})_3$ (tris(2,2,6,6-tetramethyl-3,5-heptanedionate)yttrium or « $Y(thd)_3$ ») have been finally selected.

$ZrCl_4$ powder is commercially available at high purity levels (more than 99.5%) and presents high vapor pressures (315 to 4000 Pa) in the range 200-250°C. This allows the design of a vaporization furnace working at relatively low temperature. In practice, a porous silica crucible is half filled with $ZrCl_4$ and placed in the temperature-controlled furnace (70 cm^3 inner volume). Argon carrier gas is then forced through the powder and

the $ZrCl_4$-enriched gas flows to the mixing chamber. This percolation technique ensures a good solid to gas mass transfer.

The metal-organic compound $Y(thd)_3$ is available commercially at slightly lower purity levels (more than 98%). It melts at 174°C and presents a high enough vapor pressure at temperatures greater than *ca.* 160°C. A silica boat with a small amount of $Y(thd)_3$ is placed in a second temperature-controlled furnace. Argon circulates over the powder surface, which is pasty at the selected temperatures. The $Y(thd)_3$ + Ar gas mixture is then introduced into the mixing chamber.

Oxygen and argon are added to the gas flow in the mixing chamber. Argon is used as an inert carrier gas but also to facilitate the ignition of the plasma, to improve its stability and to adjust the partial and total pressures in the deposition chamber.

Only a few grams of Zr and Y precursors are vaporized at each deposition experiment, as given by crucible mass measurements. This corresponds, in the standard conditions (see Table 1), to approximate mass loss rates of 1.4 g/h and 0.25 g/h and gaseous precursor mole fractions in the mixing chamber of about $2\ 10^{-3}$ and $1.5\ 10^{-4}$, respectively. After deposition, the crucibles with the remaining powder are removed from the furnaces, after having cooled down to room temperature, and stored until the next utilisation. Vaporization conditions for both furnaces were investigated, and charts of precursor mass loss *vs.* furnace temperature and argon flow rate were drawn.

Although both precursors are moisture sensitive, they can be stored for several months in appropriate dessicators, without significant variation of their properties. To prevent corrosion of metallic parts by hydrochloric acid (produced by the reaction of moisture with chlorides), the whole apparatus is flushed with argon after each deposition experiment and is continuously kept under vacuum. No excessive corrosion is noticed after three years operation.

The whole gas generation part, from the furnaces downwards to the injection nozzle, is heated at 250°C to avoid condensation of the gaseous precursors.

Table 1 - Experimental conditions for the deposition of ZrO_2-Y_2O_3 TBC coatings.

Parameter		Range	Standard conditions
O_2 flow rate	(sccm)	25 - 500	200
Ar total flow rate	(sccm)	50 - 1400	800
for Zr furnace	(sccm)	20 - 700	100
for Y furnace	(sccm)	10 - 140	50
Zr furnace temperature	(°C)	25 - 250	210
Y furnace temperature	(°C)	25 - 250	170
Total pressure in deposition chamber	(Pa)	13 - 1330	133
Microwave input power	(W)	0 - 1200	750
Substrate temperature	(°C)	300 - 750	400
Nozzle exit - substrate distance	(mm)	25 - 90	50
Deposition duration	(h)	0.25 - 3	1

2.2 Gas injection

The injection of the precursor gases into the deposition chamber is of primary importance as coatings with homogeneous thickness are required. This is especially the case if real complex-shaped turbine blades are to be coated. But the present laboratory-scale deposition reactor has been designed for investigations on small samples, so that this requirement is less severe. Nevertheless, both to get insight in the fluid dynamics around the sample and to prepare an up-scaling of the reactor, flow simulations in the deposition chamber have been performed [24].

The small cylindrical nozzle used by Bertrand [22] has been replaced by a conical convergent-divergent nozzle as shown on Figure 2. The nozzle has been designed using one-dimensional isentropic flow relations [26] so that a shock wave is located in the divergent part. The flow at the nozzle exit remains thus subsonic in a wide range of experimental conditions. The flow properties at that location were then used as input boundary conditions for finite element calculations [27] in the deposition chamber, neglecting the presence of Zr and Y precursors (less than 1 mol%), as illustrated on Figure 3. For some calculations, the heating of the gas by the microwave plasma was taken into account, but the numerous chemical reactions induced by the plasma were up to now neglected. These simulations will be used to optimize the deposition process, with respect to both deposition efficiency and coating homogeneity on complex-shaped substrates.

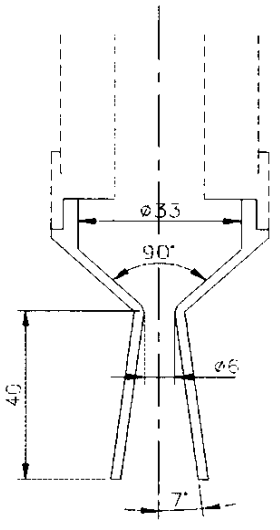

Figure 2 - Schematic view of the gas injection nozzle.

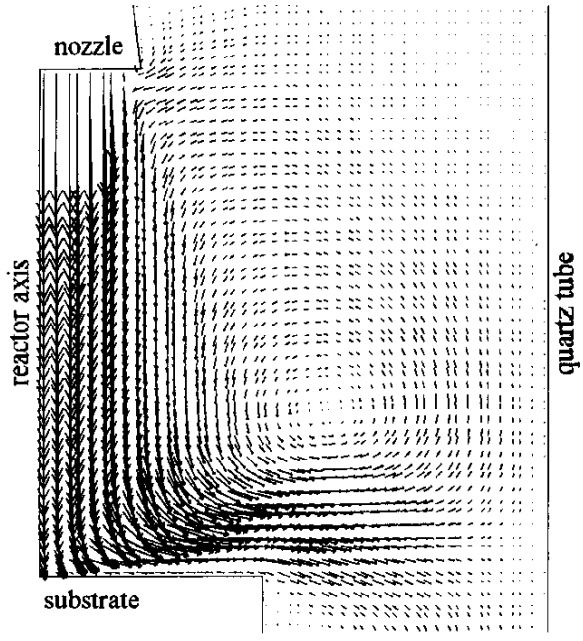

Figure 3 - Simulation of the gas flow in the deposition chamber. P = 130 Pa, total flow rate : 1000 sccm (80% Ar - 20% O_2), distance from nozzle exit to substrate : 50 mm, T_S = 400°C, input gas temperature : 220°C, no plasma.

3. RESULTS AND DISCUSSION

The structure of the ZrO_2 - (5-20wt%) Y_2O_3 coatings has been characterized using scanning electron microscopy (SEM) and X-ray diffraction (XRD ; CuKα radiation). The yttrium content in the various phases has been indirectly obtained by XRD, using the following relations obtained from Scott's measurements [28] between the $YO_{3/2}$ mole fraction, X, and the lattice parameters a and c (in angstroems) :

for $0.03 < X < 0.13$ (tetragonal phase) :

$$a_t = 5.08 + 0.358\,X \quad (1)$$

$$c_t = 5.195 - 0.31\,X \quad (2)$$

for $0.12 < X < 0.33$ (cubic phase) :

$$a_C = 5.115 + 0.16\,X. \quad (3)$$

The yttria contents will be given in Y_2O_3wt%, which is approximately equal to $YO_{3/2}$mol%. The impurity content has been measured using nuclear reaction spectroscopy (NRS) and particle-induced X-ray emission spectroscopy (PIXE), for carbon and chlorine detection (detection limits : 0.4 and 0.1at%, respectively). These techniques were also used to check the overall Y content in some coatings.

3.1 Morphology

All deposited coatings showed columnar morphology, as illustrated on Figure 4. The columns, originating from the substrate surface, exhibit conical shape, leading to domed top surface. This morphology, frequently obtained in CVD, results from the nuclei preferential growth in given directions.

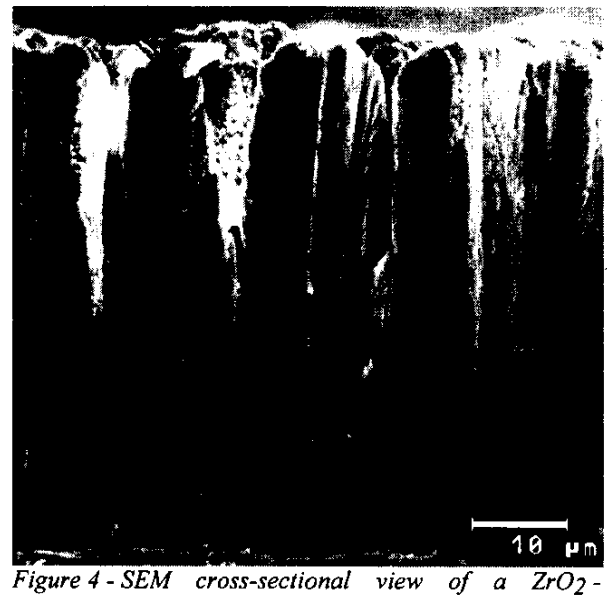

Figure 4 - SEM cross-sectional view of a ZrO_2 - 5wt% Y_2O_3 coating deposited in the standard conditions (deposition duration : 1 hour).

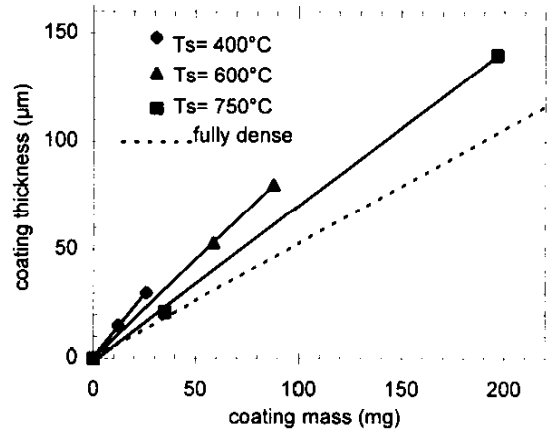

Figure 5 - Coating thickness vs. coating mass for various substrate temperatures and for a fully dense coating (with ρ = 6020 kg/m^3).

The pore volume fraction in the coating has been evaluated by the simple relation $P = 1 - \rho_{exp}/\rho_{th}$, with ρ_{exp} the experimental coating specific mass, measured as the substrate mass increase over coating volume ratio, and ρ_{th}, the specific mass of fully dense ZrO_2 - 8wt% Y_2O_3 ($\rho_{th} \approx 6020$ kg/m^3) ; because of the errors on the coating mass and volume measurements, these results are estimated to be accurate within ±10 rel%. Figure 5 shows the variation of the coating thickness *vs.* coating mass for various substrate temperatures. The slope of the straight lines is $1/(\rho_{exp}.S)$, with S the substrate surface area. This allows to calculate ρ_{exp} and P, as summarized in Table 2.

It is seen that the porosity level is highly dependent on the substrate temperature during deposition. This is a typical coating growth feature for high deposition rate processes (especially PVD), as a competition between ad-particle (atoms, molecules) arrival rate and thermally

Table 2 - Measured specific mass ρ_{exp} and pore volume fraction P, for various substrate temperatures.

Substrate temperature (°C)	ρexp (kg/m^3)	P
400	2760	54 %
600	3500	42 %
750	4420	26 %

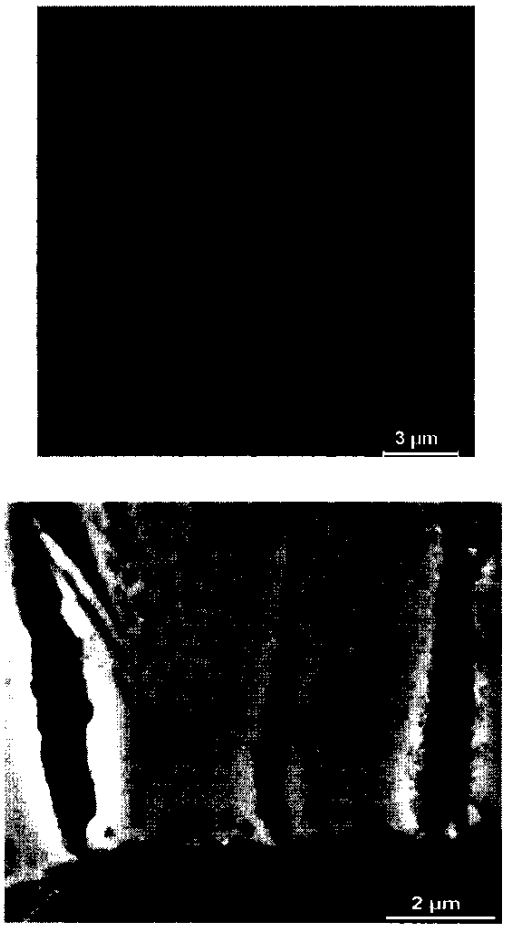

Figure 6 - SEM cross-sectional view of a coating deposited in the standard conditions (T_S = 400°C) and annealed for 24 hours at 1100°C in air : bulk of coating (top) and substrate-coating interface (bottom).

activated particle surface diffusion [29]. In the present case, the time interval between ad-particles arrival is about 20 ms, being defined as $c/2R$ with c the lattice parameter ($c \approx 5\ 10^{-10}$ m) and R the deposition rate. At low deposition temperatures, the distance travelled by the adsorbed particles by surface diffusion during that time interval is too small to allow the construction of a « perfect » crystal so that many voids (vacancy clusters or pores) are incorporated into the coating. It is seen on the SEM coating cross-sections (Figure 4) that intercolumnar porosity cannot account for the whole measured 54% pore volume fraction, showing that intracolumnar porosity exists which cannot be resolved by SEM. At higher deposition temperatures, surface diffusion becomes more important, by *ca.* one order of magnitude between 400°C and 750°C if a 1eV activation energy is assumed, so that less porous structures are allowed to grow. At high temperatures, bulk diffusion can also contribute to the elimination of porosity.

The porosity is not homogeneous throughout the coating, the first micrometers appearing to be more dense. Annealing at 1100°C in air for 24 hours produces the coalescence of the intergranular porosity which becomes observable by SEM. This sintering takes place throughout the coating, as seen on Figure 6 (bulk of coating and column base).

The deposition of highly porous coatings could have been interesting with respect to lowered thermal conductivities, if the obtained morphology had been thermally stable up to temperatures corresponding to gas turbine applications. This is clearly not the case here.

3.2 Deposition rate

The deposition rate is about 55 µm/h (48 mg/h) in the standard conditions. Figure 7 shows that the deposited zirconia amount (here at T_S = 400°C) is proportional to the vaporized precursor mass and thus to the partial pressure of zirconium compounds in the gas phase. Figure 8 shows that the substrate temperature has very little effect on the deposition rate. This indicates that the process is not controlled by surface kinetics. Further experiments are necessary to determine the limiting step of the deposition process (mass transport, gas phase reactions, ...) for various deposition conditions. Note that the analysis of the deposition mechanism is more complicated than for conventional thermal CVD, as the influence of the plasma must be taken into account.

The deposition rate depends both on the gaseous precursors flow rates (at least for $ZrCl_4$) and the overall deposition efficiency. The former is related to the vaporization capability of the $ZrCl_4$ and $Y(thd)_3$ furnaces. The $ZrCl_4$ furnace has been tested up to mass flow rates corresponding to deposition rates of 150 µm/h (about 200 mg/h ZrO_2 - Y_2O_3 deposited on the substrate, at T_S = 750°C) ; up-scaling of both furnaces should not present any problems. The latter is related first to the physical and chemical processes in the gas phase and at the gas/coating interface and secondly to the gas injection conditions and to the geometrical configuration of the deposition chamber, *i.e.* nozzle geometry, substrate size and shape, nozzle-substrate distance, *etc.* Hence, the deposition efficiencies, defined as the number of deposited Zr moles to the number of vaporized Zr moles ratio, that can be calculated from Figure 8, *i.e.* 8-10%, apply only to the current non-optimized deposition configuration. For instance, the deposition rate for a nozzle exit - substrate distance of 75 mm is the half of that at 50 mm : this is due to the fact that the flow undergoes a conical expansion in the nozzle and in the deposition chamber. An efficiency of at least 20% would be achievable after process optimization.

Most coatings were deposited at rates lower than about 80 µm/h, because beyond that value thickness

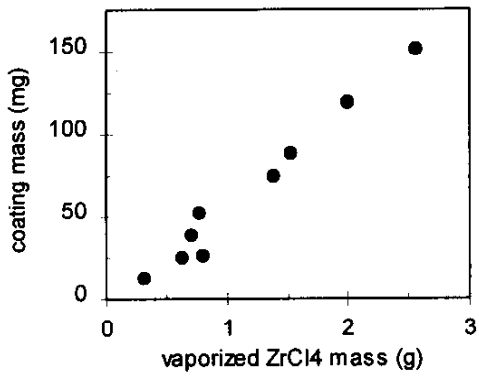

Figure 7 - Deposited zirconia mass vs. vaporized $ZrCl_4$ precursor mass. T_S = 400°C, P = 133 Pa, flow rates : direct Ar, 500-700 sccm, Zr-furnace carrier gas (Ar), 50-300 sccm, O_2, 200-300 sccm, microwave power : 400-900 W, nozzle-substrate distance : 50 mm.

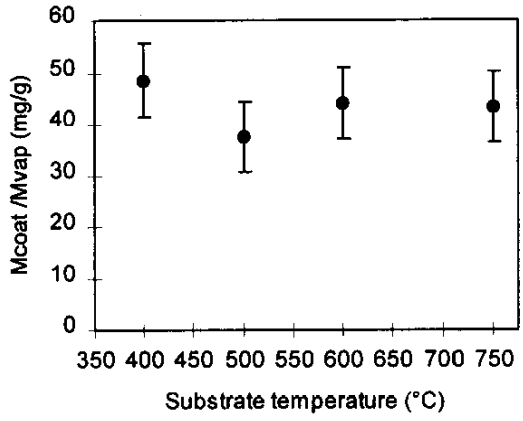

Figure 8 - ZrO_2 mass deposition rate (in g/h), normalized to the vaporized $ZrCl_4$ rate (in mg/h), as a function of substrate temperature T_S.

heterogeneity increases (the thickness ratio at substrate center and edge becoming higher than about 2, in this configuration).

3.3 Impurity content

Because these elements are present in the chloride and organo-metallic gaseous precursors, chlorine and carbon may be incorporated into the ZrO_2 - Y_2O_3 coatings. Table 3 shows the atom contents measured at two deposition temperatures. At T_S = 400°C, the C content is not negligible (even if this corresponds to only 2wt%, approximatively) and reflects the fact that the gas phase has been enriched in carbonaceous compounds, originating from the (partial) dissociation of $Y(thd)_3$ in the plasma, which where able to adsorb on the coating surface. It had not been possible to check whether the carbon is incorporated preferentially as free carbon or as a Zr compound. Nevertheless, at high deposition temperature, the C content is drastically reduced (less than 0.5wt%) probably because the kinetics of the

Table 3 - Measured C and Cl atom contents in ZrO_2 - Y_2O_3 coatings at low and high deposition temperatures.

Substrate temperature (°C)	C content (at%)	Cl content (at%)
400	6.8 ±0.5	2.0
750	1.5	< 0.1

oxidation by atomic or molecular oxygen leading to gaseous products (CO, CO_2) has become favoured.

At low deposition temperature, the coatings incorporate some chlorine. The measured content can appear to be relatively high if corrosion issues are in mind ; but it also shows how efficient the plasma decomposition and reaction processes are, by reducing the Cl:Zr atom ratio from 4:1 in the mixing chamber to about 2:30 in the coating, knowing that at T_S = 400°C thermal CVD cannot take place. For T_S = 750°C, no chlorine can be detected in the coatings, here also because reactions of chlorine compounds with oxygen leading to volatile products are favoured at that high temperature.

3.4 Crystallographic structure

Zirconia coatings, partially stabilized with yttria with mass fractions in the range 5 - 20 %, were deposited at T_S = 400°C. XRD diagrams for coatings with approximately 7, 10 and 16wt% Y_2O_3 are shown on Figure 9 (T_S = 400°C). All coatings exhibit crystallographic texture, the {100} planes being preferentially oriented parallel to the sample surface. The yttria content was deduced from the value of the *a* lattice parameter. In accordance to the phase diagram, for both ZrO_2 - 7wt% Y_2O_3 and ZrO_2 - 10wt% Y_2O_3 coatings, the main phase is the metastable non-transformable phase « *t'* » (with a small amount of monoclinic phase « *m* »), while the ZrO_2 - 16wt%Y_2O_3 coatings crystallize in the cubic phase « *c* ».

The ZrO_2 - 7wt%Y_2O_3 has been more specifically studied. After annealing at 1200°C for 24 hours in air, the texture (which is here more precisely (100)) is amplified, but from there on remains stable, as shown by further annealing for 96 hours. During this high temperature treatment, the « *t'* » phase is depleted in yttria while cubic phase is allowed to form. After 24 hour annealing, the yttria content of the « *t'* » phase is reduced to about 5wt%, to the benefits of cubic phase (or a tetragonal phase with a *c/a* ratio close to 1) with *ca.* 11wt% Y_2O_3, which is the lower limit for the existence of this phase at 1200°C. After further annealing during 96 hours, the yttria content of the « t' » phase still decreases, to about 4wt%, but it remains constant for the cubic phase. This means that in this second step, the yttria transferred from the « t' » to the « c » phase has been consumed only to allow the increase of the cubic phase volume fraction within the sample, as is observed on Figure 10. The return to thermodynamic equilibrium, by development of the cubic phase, is somewhat faster than that observed by Lelait [30] for plasma - sprayed ZrO_2 - 8wt%Y_2O_3

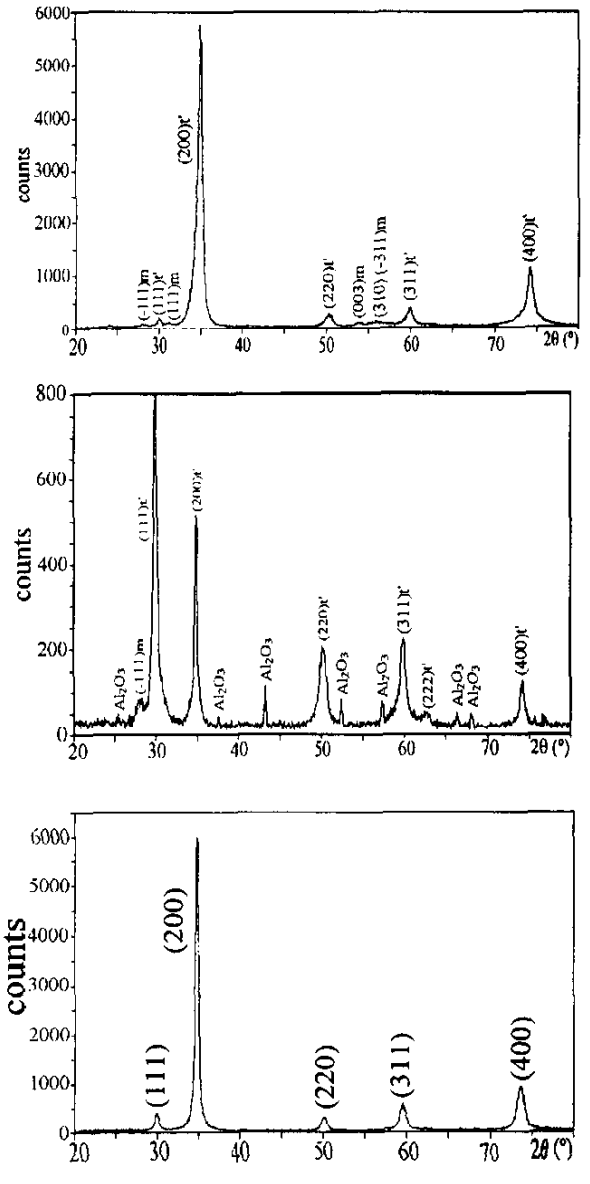

Figure 9 - XRD diagrams of as-deposited PECVD ZrO_2 - x Y_2O_3, with x = 7wt% (top), 11wt% (middle) and 16wt% (bottom). Al_2O_3 peaks are due to spalled areas (edges) on an alumina substrate.

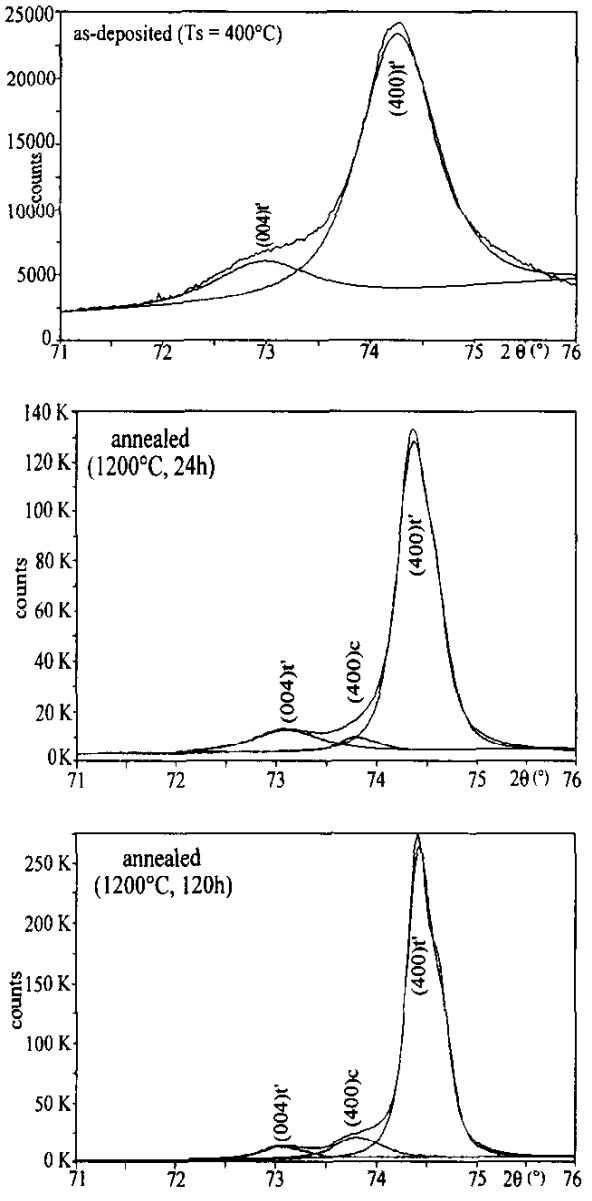

Figure 10 - {400} region of XRD diagrams for a ZrO_2 - 7wt% Y_2O_3 coating. Experimental diagrams and calculated contributions of the « t' » and « c » phases : as-deposited (top), annealed at 1200°C in air for 24 hours (middle) and 120 hours (bottom).

coatings, which appears after about 250 hours at 1200°C. This different behaviour of the PECVD sample may be explained by the high porosity level of the coating deposited at low temperarure (T_S = 400°C) : the high amount of internal surfaces thus generated may favour, comparatively to volume diffusion, the surface diffusion of Y^{3+} cations, which are responsible for the evolution of the « t' » metastable system towards thermodynamic equilibrium.

4. CONCLUSION

Plasma-assisted chemical vapor deposition has been successfully used to deposit thick (20 - 150 µm) zirconia-(5-20wt%) yttria coatings on metallic and alumina substrates, with high rates (up to 150 µm/h) at temperatures ranging from 400 to 750°C. $ZrCl_4$ and $Y(thd)_3$ were used as source materials ; vaporization, handling and storage procedures have been established for both precursors.

Morphology, impurity content and crystallographic structure of the coatings were investigated. At all deposition temperatures, the coatings exhibited columnar morphology and {100} crystallographic texture. At low substrate temperature (400°C), the pore volume fraction was high (*ca.* 50%) and the coatings incorporated some carbon and chlorine impurities, but at higher temperature (750°C), the pore volume fraction reduced to about 25% and little carbon and no chlorine were detected. It thus

appears that medium to high temperatures are unavoidable to synthesize suitable coatings for thermal barrier applications.

Metastable tetragonal « t' » phase was the major constituent of coatings with 7 and 11wt% yttria, while 16wt%-yttria coatings exhibited only the cubic phase, in accordance to the phase diagram. Annealing for 24 and 120 hours of ZrO_2 - 7wt% Y_2O_3 coating deposited at 400°C showed that cubic phase with an yttria content of about 11wt% is allowed to grow, at the expense of the « t' » phase whose yttria content diminishes to 5wt% and 4wt%. This relatively fast evolution towards thermodynamic equilibrium may be related to the high porosity level.

Work is in progress to further investigate the applicability of PECVD to coat complex-shaped substrates and to study the relationships between deposition parameter and coating properties.

ACKNOWLEDGEMENTS

This study has benefited from a partial financial support from the Délégation Générale de l'Armement (DSP and SPAé). Thorough XRD investigations performed by C. Diot and T. Ochin, as well as fruitful discussions, have been are greatly appreciated.

REFERENCES

[1] Stecura S., « Optimization of NiCrAl/ZrO_2-Y_2O_3 thermal barrier systems », NASA TM 86905 (1985).

[2] Maleto M.I., Solovjeva L.I., Turesvskaya E.P., Vorolitov K.A., Yanovskaya M.I., « Alkoxy-derived Y_2O_3-stabilized ZrO_2 thin films », Thin Solid Films 249, 1-5 (1994).

[3] Yamane H., Hirai T., « Yttria stabilized zirconia transparent films prepared by chemical vapour deposition », J. Crystal Growth 94, 880-884 (1989).

[4] Kim J.S., Marzouk H.A., Reucroft P.J., « Deposition and structural characterization of ZrO_2 and yttria-stabilized ZrO_2 films by chemical vapour deposition », Thin Solid Films 254, 33-38 (1995).

[5] Cao C.B., Wang J.T., Yu W.J., Peng D.K., Meng G.Y., « Research on YSZ thin films prepared by plasma-CVD process », Thin Solid Films 249, 163-167 (1994).

[6] Brinkman H.W., Meijerink J., de Vries K.J., Burggraaf A.J., « Kinetics and morphology of electrochemical vapour deposited thin zirconia/yttria layers on porous substrates », J. Eur. Ceram. Soc. 16, 587-600 (1996).

[7] Carter W.B., Godfrey S., « Combustion vapor deposited partially stabilized zirconia coatings », in « Elevated temperature coatings : Science and technology I », Dahotre N.B., Hampikian J.N., Stiglich J.J. Eds., The Minerals, Metals & Materials Society, 103-111 (1995).

[8] Andritschky M., Rebouta L., Teixeira V., « Corrosion and adherence of stabilized ZrO_2 coatings at high temperatures », Surf. Coat. Technol. 68/69, 81-85 (1994).

[9] Kreutz E.W., Lemmer O., Wesner D.A., Alunovic M., Erkens G., Leyendecker T., Voss A., « Electron and laser radiation as sources of zirconia film deposition », Surf. Coat. Technol. 74/75, 1005-1011 (1995).

[10] Movchan B.A., « EBPVD technology in the gas turbine industry : present and future », JOM, 40-45 (nov. 1996).

[11] Grünling H.W., Mannsmann W., « Plasma sprayed thermal barrier coayings for industrial gas turbines : morphology, processing and properties », J. Phys. IV, Colloque C7 suppl. J. Phys. III, 3, 903-912 (1993).

[12] Mévrel R., « Barrières thermiques pour aubages de moteurs aéronautiques. Etat de l'art et perspectives », La Recherche Aérospatiale 5-6, 381-392 (1996).

[13] Meier S.M., Gupta D.K., « The evolution of thermal barrier coatings in gas turbine engine applications », ASME J. Eng. Gas Turbines Power 116, 250-257 (1994).

[14] Osyka A.S, Rybnikov A.I., Leontiev S.A., Nikitin N.V., Malashenko I.S., « Experience with metal/ceramic coating in stationary gas turbines », Surf. Coat. Technol. 76/77, 86-94 (1995).

[15] Parker D.W., « Improving thermal efficiency with ceramic thermal barrier coatings », Proceed. of the Internat. Symp. on Developments and Applications of Ceramics and New Metal Alloys, Quebec City, Canada, aug. 29 - sept. 2, 1993, 603-613.

[16] Minh N.Q., « Ceramic fuel cells », J. Am. Ceram. Soc. 76(3), 563-588 (1993).

[17] « Thermal Barrier Coating Workshop '95 » (Cleveland, Ohio, USA, mar. 27-29, 1995), NASA-CP-3312 (1995).

[18] « Thermal Barrier Coating Workshop 1997 » (Cincinnati, USA, may 19-11, 1997)

[19] DeMasi-Marcin J.T., Gupka D.K., « Protective coatings in the gas turbine engine », Surf. Coat. Technol. 68/69, 1-9 (1994).

[20] Rossnagel S.M., Cuomo J.J., Westwood W.D., Eds., « Handbook of plasma processing technology », Noyes Publications, ISBN-0-8155-1220-1 (1990).

[21] Seiberras G., « Réalisation et caractérisation de revêtements de zircone obtenus par dépôt chimique en phase vapeur assisté par un plasma miro-onde », Thèse de Doctorat, Université Paris 11-Orsay, mar. 24th, 1994.

[22] Bertrand G., Mévrel R., « Zirconia coatings realized by microwave plasma-enhanced chemical vapor deposition », Thin Solid Films 292, 241-246 (1997).

[23] Gavillet J., Belmonte T., Hertz D., Michel H., « Low temperature zirconia thin film synthesis by a chemical vapour deposition process involving $ZrCl_4$ and O_2-H_2-Ar microwave post-discharges. Comparison with a conventional CVD hydrolysis process », Thin Solid Films 301, 35-44 (1997).

[24] Chevillard S., « Etude d'un procédé de dépôt chimique en phase vapeur assisté par un plasma micro-

onde pour la réalisation de revêtements de zircone yttriée », Thèse de Doctorat, Université Paris 11-Orsay, feb. 11th, 1997.

[25] Chevillard S., Vidal-Sétif M.H., Drawin S., « Yttria partially stabilised zirconia coatings by microwave plasma enhanced CVD (MPECVD) », 10th Intern. Colloq. on Plasma Processes, Antibes (France), jun. 11-15, 1995, Suppl. Revue « Le Vide : science, technique et applications » 275, 431-434 (1995).

[26] Yahya S.M., « Fundamentals of compressible flows », Halsted Press (John Wiley & Sons, 1982).

[27] Fluxexpert code, DT2I, Chemin des Prèles, 38240 Meylan ZIRST (France).

[28] Scott M.G., « Phase relationship in the zirconia-yttria system », J. Mater. Sci. 10, 1527-1535 (1975).

[29] Yang Y.G., Johnson R.A., Wadlay H.N.G., « A Monte Carlo simulation of physical vapor deposition of nickel », Acta Mater. 45(4), 1455-1468 (1997).

[30] Lelait L., « Etude microstructurale fine de revêtements céramiques de type barrière thermique ; incidence sur la résistance thermomécanique de ces revêtements » Thèse de Doctorat, Université Paris 11-Orsay, 1994.